doi:10.1246/cl.2010.1114

Published on the web September 11, 2010

In Situ Electrodeposited FePt Nanoparticles for Oxygen Reduction with High Activity and Long-term Stability

Di Liu, Yang Tian,* Anwei Zhu, and Yongping Luo
Department of Chemistry, Tongji University, Siping Road 1239, Shanghai 200092, P. R. China

(Received July 8, 2010; CL-100616; E-mail: yangtian@mail.tongji.edu.cn)

In this letter, a low-cost, procedurally simple, and environmentally friendly strategy has been developed for in situ electrodeposition of FePt nanoparticles on L-cysteine-modified gold electrode surfaces. The as-prepared 20 nm FePt nanoparticles show high activity toward ORR, which is comparable with that of commercial Pt catalyst. In addition, the electrodeposited FePt nanoparticles exhibit relatively long-term stability, possibly because the alloyed Fe may prevent the dissolution of small Pt nanoparticles in the ORR.

Polymer electrolyte fuel cells (PEFCs) have attracted lots of interest as a sustainable power source for transport, stationary, and portable applications because of their high efficiency and low emissions. A large amount of effort has been devoted to development of efficient cathodic electrocatalysts, because a sluggish oxygen reduction reaction (ORR) causes a large overpotential at low temperatures.[1–6] To date, the best materials for the ORR catalysis are still platinum or its alloys. Recently, enhanced ORR activities have been widely reported by using Pt alloys, such as FePt, CoPt, and NiPt.[7–9] We have also successfully produced amorphous FeNiPt nanostructures and developed electrocatalysis.[10] Recently, nanoalloy catalysts have been synthesized by various chemical methods and then confined onto electrode surfaces by organic agents such as Nafion to stabilize the nanoparticles. In contrast with all the physical deposition processes, electrochemical deposition offers a unique way for in situ generating alloy nanoparticles directly onto electrode surfaces with long-term stability. In this letter, a low-cost, facile, and environmentally friendly strategy has been developed for in situ fabrication of Pt nanoalloys. As a model of Pt nanoalloys, ca. 20 nm FePt alloyed nanoparticles have been successfully electrodeposited by chronoamperometry onto L-cysteine (Cys)-modified gold electrode surfaces. Experimental results revealed that the FePt nanoparticles can lower the OH coverage on Pt and subsequently improve both activity and stability of electrocatalyst for O_2 reduction.

Dihydrogen hexachloroplatinate ($H_2PtCl_6 \cdot 6H_2O$, 99%) and L-cysteine (Cys, $C_3H_7NSO_2$, 99%) were purchased from Alfa Aesar. Iron(II) chloride ($FeCl_2 \cdot 4H_2O$, 98%) was purchased from Sinopharm Chemical Reagent Co., Ltd. Pt reference catalysts for fuel cells with a diameter of 2.5 nm were purchased from E-TEK. Nafion solution (5 wt %) was received from Sigma and diluted with ethanol. Indium tin oxide (ITO)-coated glass plates with a square resistance of ca. $10\,\Omega\,cm^{-2}$ were purchased from Shenzhen Nanbo Display Technology Co.

A gold disk electrode (1.6 mm in diameter) was first polished with alumina slurries and then cleaned by sonication in Milli-Q water. Then the electrode was modified with Cys by immersing into an aqueous solution of 0.2 mM Cys for ca. 30 min at room temperature. The Cys-modified gold electrode was immersed into a mixed solution of $FeCl_2 \cdot 4H_2O$ (2.5 mM) and $H_2PtCl_6 \cdot 6H_2O$ (2.5 mM). The present FePt nanoparticles were electrodeposited by chronoamperometry with first scan stepping from 0.8 to −0.3 V, followed by the second scan from 0.8 to −0.4 V, and then from 0.8 to −0.5 V, 0.8 to −0.55 V, 0.8 to −0.6 V, 0.8 to −0.7 V, 0.8 to −0.75 V, and last scan from 0.8 to −0.8 V, in turn, with pulse width of 5 s. The Pt/Fe atom ratio was optimized as ca. 86/14.

The morphology was characterized by using a scanning electron microscope (SEM) Quanta 200 FEG (FEI Co.). X-ray photoelectron spectroscopy (XPS) experiments were carried out on a RBD upgraded PHI-5000C ESCA system (Perkin-Elmer) with Mg Kα radiation ($h\nu = 1253.6$ eV). Binding energies were calibrated by using the containment carbon ($C_{1s} = 284.6$ eV). An ITO glass plate was electrodeposited with gold and employed as substrate for the above characterizations.

Before recording the voltammograms, the modified electrode surface was cleaned in N_2-saturated 0.5 M H_2SO_4 by cycling between −0.2 and 1.3 V (vs. Ag|AgCl) until steady cyclic voltammograms (CVs) were observed. Cyclic voltammetry and rotating disk voltammetry were performed using a computer-controlled CHI 760 electrochemical workstation (CH Instrument Co.) and an adjustable speed rotator (Pine Instrument Co.). The electrochemical surface area (ECSA) was calculated by integrating the area under the curve in the hydrogen adsorption range between 0.05 and 0.4 V for the backward sweep in the CV. All oxygen reduction reaction (ORR) tests were conducted at ambient room temperature.

Figure 1A shows SEM image of the as-prepared FePt nanoparticles. A good distribution of ca. 20 nm spherical particles over the gold substrate was observed. XPS spectra for the FePt nanostructures are also depicted in Figures 1B–1D, in which the numbers of emitted photoelectrons are given as a function of binding energy up to 1100 eV. As shown in Figure 1B, four photoemission peaks were clearly observed for Fe2p, Pt4f, C1s, and O1s, while the emission from the inelastic collisions of photoelectrons gave rise to a general background. Two sharp peaks located at ca. 71.2 and ca. 74.6 eV, as shown in Figure 1C, were ascribed to the spin–orbit splitting of $4f_{7/2}$ and $4f_{5/2}$ for magnified Pt4f. The spin–orbit doublet splitting value of the 4f core level estimated to be ca. 3.4 eV, corresponding to the difference of binding energies (BE) between $4f_{7/2}$ and $4f_{5/2}$, indicates that metallic Pt is dominant in the Pt–Fe nanostructures.[11] As demonstrated in Figure 1D, two peaks located at ca. 706.8 and ca. 720.1 eV owing to the spin–orbit doublet splitting of $2p_{3/2}$ and $2p_{1/2}$ were in an agreement with the values reported previously for metallic Fe, although Fe is easy to be partly oxidized and the feature peak of Fe becomes broad.[12] Thus, we can conclude that not only Pt but also Fe are reduced and both metals are in their metallic state in the Pt–Fe nanostructures.

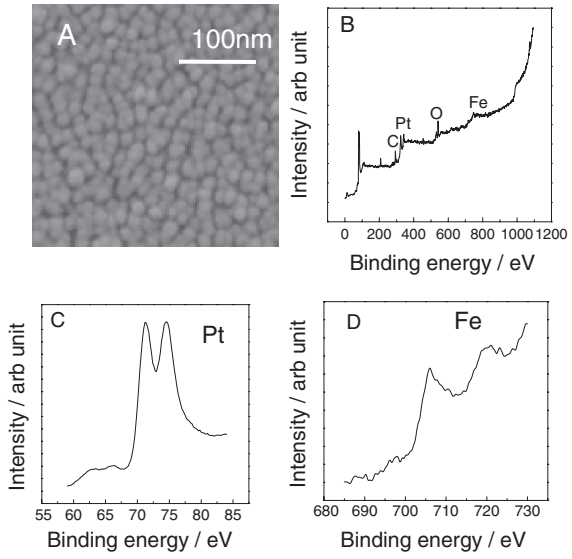

Figure 1. (A) SEM image of FePt nanoparticles. X-ray photoelectron spectra (B) for FePt nanoparticles, (C) for Pt in FePt nanoparticles, and (D) for Fe in FePt nanoparticles. The horizontal axes represent the binding energy corrected by that of C1s.

The hydrodynamic voltammograms for the ORR were obtained at the electrode in O_2-saturated 0.5 M H_2SO_4 solution at a potential scan rate of 50 mV s^{-1}, as shown in Figure 2A. From the voltammograms, the limiting current densities (J_L) were plotted as a function of $\omega^{1/2}$ and given in the inset of Figure 2A. The experimental values fall on a straight line passing through the origin, suggesting that the reaction is controlled by the diffusion of O_2 to the electrode surface. According to Levich equation, the number of electrons involved in the O_2 reduction was calculated to be 4.[13] The slope of the experimental line was obtained as 0.395 mA cm^{-2} (rad $s^{-1})^{-1/2}$ which is consistent with that of the theoretical line for $n = 4$ (0.40 mA cm^{-2} (rad $s^{-1})^{-1/2}$), confirming that the ORR at the alloy electrode proceeds through a four-electron pathway. The area-specific current density (J_K), which represents the intrinsic activity of the catalysts, was calculated using Koutecky–Levich equation.

$$\frac{1}{J} = \frac{1}{J_K} + \frac{1}{J_D} = \frac{1}{J_K} + \frac{1}{0.62nFC_O D_O^{2/3} \upsilon^{-1/6} \omega^{1/2}}$$
$$= \frac{1}{J_K} + \frac{1}{B\omega^{1/2}}$$

As shown in Figure 2B, J_K was estimated to be 1855 μA cm^{-2} at 0.75 V for the FePt nanoparticles, which is a little larger than that for the commercial Pt catalyst (ca. 1300 μA cm^{-2}),[14,15] and is comparable with those at Pt-on-Pd alloy[16] and Pt_3Co nanostructures.[14]

In order to find the origin of the ORR enhancement by using FePt nanoparticles, CVs of FePt nanoparticles and commercial Pt nanoparticles were measured in H_2SO_4 solution under N_2 bubbling. The CV peak associated with the formation of oxygenated adsorbates (0.8–0.9 V) at the low-cost FePt surface showed a comparable potential with that at commercial Pt nanoparticle surface. The increased electronic interaction of O_2 with the bimetallic electrode surface promotes the adsorption of

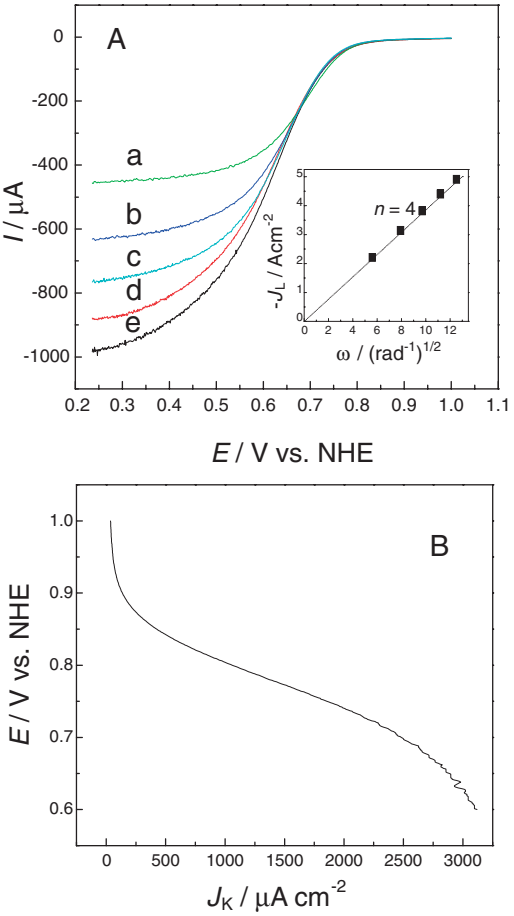

Figure 2. (A) Hydrodynamic voltammograms obtained at the FePt rotated disk electrode (RDE) in O_2-saturated 0.5 M H_2SO_4 solution. Specified rotating rates: (a) 1200, (b) 1500, (c) 1800, (d) 2100, and (e) 2400 rpm. Inset: Levich plot for the ORR at the RDE in O_2-saturated 0.5 M H_2SO_4 solution. The values of J_D were obtained from the voltammograms shown in Figure 2A. The solid circles represent the experimental values while the dotted lines correspond to the theoretically predicted lines for four electron reductions of O_2. (B) Tafel plot of kinetically controlled ORR currents obtained at the FePt nanoparticles with rotating rate of 1200 rpm.

O_2 molecules, and thus may facilitate the rupture of the bonds in O_2 resulting in an increase of the ORR activity.

The stability of the in situ prepared FePt catalyst was evaluated by applying linear potential sweeps between 0.6 and 1.0 V as previously reported.[16] Figure 3 shows CVs obtained at (A) commercial Pt nanoparticles and (B) FePt nanoalloys before (a) and after (b) 30000 cycles scanned in H_2SO_4. The electrochemical surface area (ECSA) was calculated by integrating the area under curve in the hydrogen adsorption range between 0.05 and 0.4 V for the backward sweep in the CV. The commercial Pt nanoparticles lost ca. 26% of the initial ECSA and showed a large decrease of 29 mV in the half-wave potential after 30000 cycles. However, the FePt nanoparticles were observed to be quite stable with a loss of only ca. 14% initial ECSA and a small degradation of 11 mV in the half-wave potential after the same examination. More importantly, the shape of CV obtained at

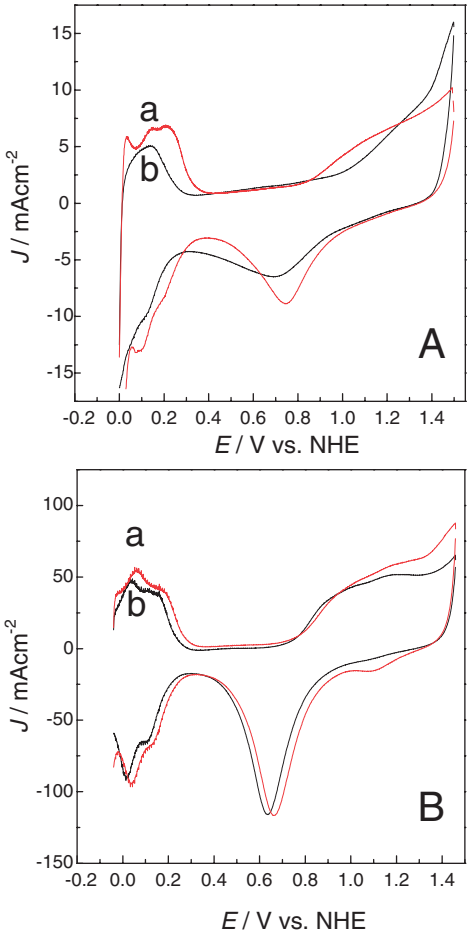

Figure 3. CVs in 0.5 M H_2SO_4 solution at scan rate of 100 mV s^{-1} for (A) Pt catalyst and (B) FePt nanocatalyst before (a) and after (b) 30000 cycles.

commercial Pt nanoparticles greatly changed, compared with that at FePt nanoparticles, suggesting that Pt nanocatalysts were easier to be poisonous and lost more electrocatalytic activity than FePt nanoparticles. The developed electrocatalytic stability may be ascribed to the Fe alloyed with Pt catalyst, which prevents the poisoning and dissolution of small Pt nanoparticles in the ORR process.

FePt alloyed nanoparticles have been successfully prepared by a low-cost and procedurally simple in situ electrodeposited strategy. Electrochemical measurements indicate that the as-prepared FePt nanoparticles exhibit comparable ORR catalytic activity to commercial Pt nanoparticles, because the increased electronic interaction of O_2 molecule with the bimetallic electrode surface promotes the adsorption of O_2 molecules and thus facilitates the rupture of the bonds in O_2 molecule resulting in an increase of the ORR activity. In addition, the alloyed metallic Fe may prevent dissolution of the small Pt nanoparticles in the ORR, thus the present catalyst shows a long-term stability. This investigation opens up a novel way to designing and developing an in situ electrodeposited method for preparation of fuel cell catalysts with both excellent activity and stability.

This work is financially supported by National Natural Science Foundation of China (No. 20975075) and Nanometer Science Foundation of Shanghai (No. 0952nm04900). Tongji University is also greatly acknowledged.

References

1 E. Antolini, J. R. C. Salgado, M. J. Giz, E. R. Gonzalez, *Int. J. Hydrogen Energy* **2005**, *30*, 1213.
2 T.-Y. Jeon, S. J. Yoo, Y.-H. Cho, K.-S. Lee, S. H. Kang, Y.-E. Sung, *J. Phys. Chem. C* **2009**, *113*, 19732.
3 M. S. El-Deab, T. Sotomura, T. Ohsaka, *Electrochem. Commun.* **2005**, *7*, 29.
4 M. S. El-Deab, T. Ohsaka, *Angew. Chem., Int. Ed.* **2006**, *45*, 5963.
5 L. Q. Mao, D. Zhang, T. Sotomura, K. Nakatsu, N. Koshiba, T. Ohsaka, *Electrochim. Acta* **2003**, *48*, 1015.
6 P. Yu, J. Yan, H. Zhao, L. Su, J. Zhang, L. Q. Mao, *J. Phys. Chem. C* **2008**, *112*, 2177.
7 S. Chen, P. J. Ferreira, W. C. Sheng, N. Yabuuchi, L. F. Allard, Y. Shao-Horn, *J. Am. Chem. Soc.* **2008**, *130*, 13818.
8 H. Yano, M. Kataoka, H. Yamashita, H. Uchida, M. Watanabe, *Langmuir* **2007**, *23*, 6438.
9 S. Mukerjee, S. Srinivasan, M. P. Soriaga, J. McBreen, *J. Electrochem. Soc.* **1995**, *142*, 1409.
10 M. Wen, H. Q. Liu, F. Zhang, Y. Zhu, D. Liu, Y. Tian, Q. Wu, *Chem. Commun.* **2009**, 4530.
11 W. Yang, X. Wang, F. Yang, C. Yang, X. Yang, *Adv. Mater.* **2008**, *20*, 2579.
12 S. Maldonado, K. J. Stevenson, *J. Phys. Chem. B* **2005**, *109*, 4707.
13 M. R. Miah, T. Ohsaka, *Electrochim. Acta* **2009**, *54*, 5871.
14 V. R. Stamenkovic, B. S. Mun, K. J. J. Mayrhofer, P. N. Ross, N. M. Markovic, *J. Am. Chem. Soc.* **2006**, *128*, 8813.
15 J. L. Fernández, V. Raghuveer, A. Manthiram, A. J. Bard, *J. Am. Chem. Soc.* **2005**, *127*, 13100.
16 Z. M. Peng, H. Yang, *J. Am. Chem. Soc.* **2009**, *131*, 7542.

